Polymer Bulletin
https://doi.org/10.1007/s00289-025-06032-7

ORIGINAL PAPER

Kinetic modeling of the synthesis of styrene–DVB resins for estimating chain density distribution

Leandro G. Aguiar[1] · Maria L. T. Reis[1] · William M. Godoy[1]

Received: 17 January 2025 / Revised: 14 July 2025 / Accepted: 6 September 2025

Abstract

A cross-linking copolymerization model based on species and sequences balance was developed and applied to styrene-based resins with 1–25% divinylbenzene (DVB). The swelling indices of these resins were estimated using a modified Flory–Rehner equation. The chain density was calculated as a function of the radius of gyration of sequences between cross-links, employing the Flory exponent as an adjustable parameter. The mathematical model was successfully validated against morphology data, yielding an average R^2 of 0.936. The model provided the fraction of linear chains and the distribution of sequences between cross-links. This distribution facilitated the calculation of swelling index distribution along the resin, following a logarithmic function of M_C with an R^2 of approximately 0.920. The results suggest that the radius of gyration equation $R_g = 0.03 M_{cr}^{\alpha}$ is applicable for chain segments between cross-links (L_{Er}) in sulfonated styrene–DVB resins. For lightly cross-linked sulfonated resins (1.5–2.5% DVB), water could be considered a theta solvent based on the coiling factors identified ($\alpha \approx 0.5$). At higher DVB percentages, the coiling behavior resembled that of polystyrene in apolar media ($\alpha \approx 0.6$), aligning with literature reports.

Keywords Chain density · Resin · Modeling · Copolymerization

List of symbols

A_{12}	Solubility term (MPa)
CLP	Cross-linking point (Dimensionless)
Cy_r	Cyclic chain containing r units (g mol^{-1})
F	Polymer fragment (g mol^{-1})
f	Initiator efficiency (Dimensionless)
f_v	Fraction of swollen polymer (Dimensionless)
I	Initiator concentration (mol L^{-1})

✉ Leandro G. Aguiar
leandroaguiar@usp.br

[1] Lorena School of Engineering, University of São Paulo, Lorena, Brazil

Published online: 19 September 2025

IERs	Ion exchange resins (Dimensionless)
k_{cyc}	Cyclization constant (s^{-1})
K	Ratio $\frac{v_R}{v_P}$ (Dimensionless)
k_d	Initiator decomposition constant (s^{-1})
k_{I1}	Styrene initiation constant (L mol^{-1} s^{-1})
k_{I2}	DVB initiation constant (L mol^{-1} s^{-1})
k_{p1}	Styrene propagation constant (L mol^{-1} s^{-1})
k_{p2}	DVB propagation constant (L mol^{-1} s^{-1})
k_{P3}	PDB propagation constant (L mol^{-1} s^{-1})
k_t	Termination constant (L mol^{-1} s^{-1})
L_{Ar}	Concentrations of sequences containing *r* styrene units connecting a PDB to a radical center (mol L^{-1})
L_{Br}	Concentration of sequences containing *r* styrene units connecting two PDBs (mol L^{-1})
L_{Cr}	Concentration of sequences containing *r* styrene units connecting a cross-linked unit to a radical center (mol L^{-1})
L_{Dr}	Concentration of sequences containing *r* styrene units connecting a PDB to a cross-linked unit (mol L^{-1})
L_{Er}	Concentration of sequences containing *r* styrene units connecting two cross-linked units (mol L^{-1})
M_1	Styrene concentration (mol L^{-1})
M_2	DVB concentration (mol L^{-1})
M_C	Molecular weights between cross-links (g mol^{-1})
m_P	Polymer mass (g)
m_S	Solvent mass (g)
M_{sty}	Molecular weight of styrene (g mol^{-1})
M_w	Molecular weight (g mol^{-1})
N_A	Avogadro's number (Molecule mol^{-1})
P	Dead polymer (mol L^{-1})
PCD	Polymer chain density (nm nm^{-3})
PDB	Pendant double bonds concentration (mol L^{-1})
P_L	Concentration of linear polymer chain (mol L^{-1})
r	Number of units between cross-links (r.u.)
R	Gases constant (atm L K^{-1} mol^{-1})
$R^{\cdot}$	Total radicals' concentration (mol L^{-1})
$R^{\cdot}_0$	Primary radicals' concentration (mol L^{-1})
R_g	Radius of gyration (nm)
$R^{\cdot}_L$	Concentration of linear radicals (mol L^{-1})
r_{max}	Maximum *r* considered in the copolymerization modeling (r.u.)
$R^{\cdot}_n$	Polymeric radical containing *n* units (mol L^{-1})
$R^{\cdot}_S$	Concentration of radicals containing only styrene units (mol L^{-1})
Sw	Swelling Index (Dimensionless)
T	Temperature (K)
V_1	Molar volume of solvent (cm^3 mol^{-1})
V_P	Polymer volume (cm^3)

w_P Weight fraction of occluded polystyrene in the gel (Dimensionless)
w_R Weight fraction of rubber in the gel (Dimensionless)
$Y_{LE,r}$ Fraction of L_{Er} among all L_E (mol L_{Er} (mol total L_E)$^{-1}$)

Greek letters

α Coiling factor (Dimensionless)
β Constant (Dimensionless)
δ_R Solubility parameter of the resin (MPa$^{0.5}$)
δ_s Solubility parameter of the solution (MPa$^{0.5}$)
μ_P Polystyrene–solvent interaction factor (Dimensionless)
μ_R Rubber–solvent interaction factor (Dimensionless)
ρ_P Occluded polystyrene density (kg dm^{-3})
ρ_{PS} Sulfonated polystyrene density (kg dm^{-3})
ρ_R Resin density (kg dm^{-3})
ρ_s Solution density (kg dm^{-3})
v_0 Volume fraction of dissolved polymer in the supernate (Dimensionless)
v_P Volume fraction of polystyrene in the swollen occluded polystyrene (Dimensionless)
v_R Volume fraction of rubber in the swollen rubber network (Dimensionless)
$\varnothing_r$ Sequence diameter (Molecule mol^{-1})
φ Density of swollen polymer (g cm^3)

Introduction

Over the last few decades, scientists have been working on the development of environmentally friendly processes by substituting harmful compounds and adopting cleaner procedures. Catalysis, one of the foundational pillars of green chemistry, has been the subject of numerous studies, particularly regarding catalyst recovery and recycling [1, 2]. In this context, heterogeneous catalysts are often highlighted over their homogeneous counterparts. Industrially, solid catalysts are preferred, utilizing a support material with immobilized catalytic sites. These solid catalysts can be metallic, silica-supported, or polymer-supported. The latter, known as ion exchange resins (IERs), are applied not only in acid–base catalysis [3] but also in water purification [4], metal recovery and separation [5, 6], ion substitution [7], sensors, and solid electrolytes [8]. Most IERs are made from styrene-based polymers cross-linked with varying percentages of divinylbenzene (DVB), resulting in different properties such as sulfonic group content (–SO_3H), porosity, and surface area. Texturally, IERs can be classified into two types: gel-type resins and macroreticular resins. Gel-type resins exhibit microporosity only after swelling, with their interiors remaining inaccessible in the unswollen or dry state. In contrast, macroreticular resins maintain stable meso- and macropores even when dry, in addition to micropores generated by the swelling of their polymeric skeleton [9, 10]. This information is crucial when using the resin as a catalyst, as the density of polymer chains and swelling behavior directly impact the accessibility to catalytic sites. Recent studies have evaluated the effect of DVB content [11] and the resulting degree of cross-linking on the reactivity

of IERs through copolymerization modeling [12]. In these studies, the concept of chain sequences (styrene units between two groups in the copolymer's structure) was introduced to describe the accessibility to catalytic sites in resins with different DVB percentages. It is well known that polymer chain density (PCD) distribution along the resin can be determined by inverse steric exclusion chromatography [13]. However, to the best of our knowledge, there are no studies on predicting PCD based on the synthesis conditions of the resin.

The present study describes a copolymerization model based on the balance of species and sequences to predict the polymer chain density of styrene–DVB resins as a function of DVB content.

Mathematical modeling

Copolymerization mechanism

The chain densities of various ion exchange resins result from the proportion of monomers and the respective kinetics of copolymerization during their synthesis. A copolymerization model, previously developed in earlier studies [11, 12], has been refined in this work by incorporating cyclization reactions and occluded linear chains. The model assumptions and an illustration of the species and sequences are presented in Fig. 1.

Assumptions:

- The sequence distributions are assumed to be identical in both soluble and gel polymers.
- Only mono-radical sequences are considered.
- Terminal model is applied.

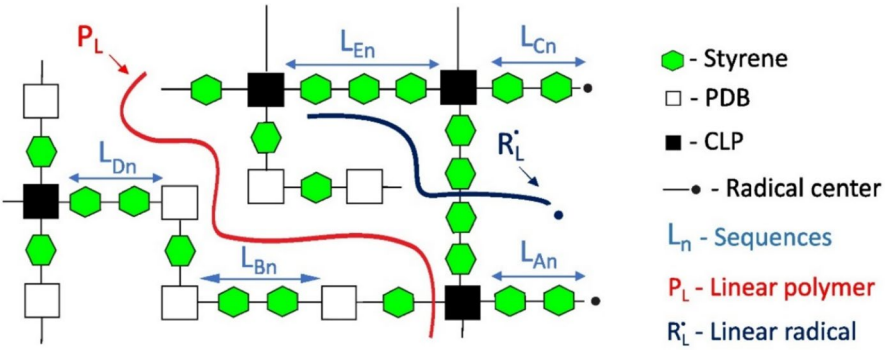

Fig. 1 Scheme of the copolymerization model. $R_L^{\cdot}$, Linear radical; P_L, Linear polymer entrapped in the polymer network; PDB, pendant double bond; CLP, cross-linking point; L_{Ar}, sequence connecting a PDB to a radical center through r units; L_{Br}, sequence connecting two PDBs through r units; L_{Cr}, sequence connecting a CLP to a radical center through r units; L_{Dr}, sequence connecting a CLP to a PDB through r units; L_{Er}, sequence connecting two CLPs through r units [11, 12]

Balance of species

The copolymerization model was formulated based on the balance of species and sequences. Table 1 outlines the free radical steps involved in the styrene–divinylbenzene copolymerization, which is the manufacturing process for most commercial acidic polymeric resins.

The balance of species is described below (refer to the symbology section for definitions of the variables).

$$\frac{\mathrm{d}I}{\mathrm{d}t} = -k_d I \tag{1}$$

$$\frac{\mathrm{d}R_0^{\cdot}}{\mathrm{d}t} = 2fk_d I - k_{I1}R_0^{\cdot}M_1 - k_{I2}R_0^{\cdot}M_2 - k_{P3}R_0^{\cdot}\mathrm{PDB} - k_t R_0^{\cdot}\left(R_0^{\cdot} + R^{\cdot}\right) \tag{2}$$

$$\frac{\mathrm{d}R^{\cdot}}{\mathrm{d}t} = k_{I1}R_0^{\cdot}M_1 + k_{I2}R_0^{\cdot}M_2 + k_{P3}R_0^{\cdot}\mathrm{PDB} - k_t R^{\cdot 2} \tag{3}$$

$$\frac{\mathrm{dPDB}}{\mathrm{d}t} = k_{I2}R_0^{\cdot}M_2 + k_{P2}R^{\cdot}M_2 - k_{P3}\mathrm{PDB}\left(R_0^{\cdot} + R^{\cdot}\right) - \sum_{r=3}^{n_{\max}} k_{\mathrm{cyc}}L_{Ar} \tag{4}$$

Table 1 Styrene–divinylbenzene copolymerization steps

Reaction	Chemical equation
Initiator decomposition	$I \xrightarrow{k_d} 2R_0^{\cdot}$
Styrene Initiation	$R_0^{\cdot} + M_1 \xrightarrow{k_{I_1}} R_{L1}^{\cdot}$
Divinylbenzene initiation	$R_0^{\cdot} + M_2 \xrightarrow{k_{I_2}} R_1^{\cdot} + \mathrm{PDB}$
PDB initiation	$R_0^{\cdot} + \mathrm{PDB} \xrightarrow{k_{P_3}} R_n^{\cdot}$
Styrene propagation*	$R_n^{\cdot} + M_1 \xrightarrow{k_{P_1}} R_{n+1}^{\cdot}$
Divinylbenzene propagation*	$R_n^{\cdot} + M_2 \xrightarrow{k_{P_2}} R_{n+1}^{\cdot} + \mathrm{PDB}$
PDB propagation*	$R_n^{\cdot} + \mathrm{PDB} \xrightarrow{k_{P_3}} R_{n+1}^{\cdot}$
Termination*	$R_m^{\cdot} + R_n^{\cdot} \xrightarrow{k_t} P_{n+m}$
	$R_0^{\cdot} + R_n^{\cdot} \xrightarrow{k_t} P$
	$R_0^{\cdot} + R_0^{\cdot} \xrightarrow{k_t} P$

I: Initiator, $R_0^{\cdot}$: primary radical, M_j: monomer of type j, $R_n^{\cdot}$: polymeric radical containing n units ($R_n^{\cdot}$ can be cross-linked or linear ($R_L^{\cdot}$) radicals), PDB: pendant double bond, P: dead polymer, k_d to k_t: rate constants of the reactions (the numerical values used can be found in a previous work) [11]

$$\frac{dM_1}{dt} = -k_{I1}R_0^{\cdot}M_1 - k_{P1}R^{\cdot}M_1 \tag{5}$$

$$\frac{dM_2}{dt} = -k_{I2}R_0^{\cdot}M_2 - k_{P2}R^{\cdot}M_2 \tag{6}$$

$$\frac{dP}{dt} = \frac{k_t}{2}R^{\cdot 2} + k_tR_0^{\cdot}R^{\cdot} \tag{7}$$

Here, f represents the initiator efficiency, accounting for the cage effect during the initiator decomposition step, and $R^{\cdot}$ denotes the concentration of all polymer radicals. Among the five sequences, only L_{Ar} can undergo cyclization because it contains both a pendant double bond (PDB) and a radical center. Thus, the term $\sum_{r=3}^{n_{\max}} k_{\text{cyc}}L_{Ar}$ represents the consumption of L_{Ar} due to cyclization for r = 3 to $n_{\max}$. The summation begins at $r = 3$ since steric hindrance prevents the formation of smaller rings with fewer than three units [14].

To estimate the content of soluble chains occluded within the polymer network, balances for linear chains ($R_L^{\cdot}$ and P_L) were conducted as follows.

$$\frac{dR_L^{\cdot}}{dt} = k_{I1}R_0^{\cdot}M_1 - k_{P2}R_L^{\cdot}M_2 - k_{P3}R_L^{\cdot}\text{PDB} - k_tR_L^{\cdot 2} - k_tR_L^{\cdot}\left(R_0^{\cdot} + R^{\cdot}\right) \tag{8}$$

$$\frac{dP_L}{dt} = \frac{k_t}{2}R_L^{\cdot 2} + \frac{k_t}{2}R_L^{\cdot}R_0^{\cdot} \tag{9}$$

The fraction of occluded soluble chains can be determined using Eq. 10.

$$w_p = \frac{P_L}{P} \tag{10}$$

Here, $R_L^{\cdot}$ represents the concentration of linear radicals, while P_L and P denote the concentrations of linear and total polymer chains, respectively. The copolymerization rate constants were obtained from the literature [14].

The consideration of only linear styrene-made chains for the calculation of occluded soluble chains (Eqs. 8–10) is a simplification related to the gelation issue. The current copolymerization model does not distinguish whether the sequences belong to the sol or gel phase. Therefore, in this approach, linear styrene-made chains ($R_L^{\cdot}$ and P_L) are the only sequences that can be confidently assumed to remain in the sol phase.

Once a DVB monomer is incorporated into a linear sequence, it forms an L_A sequence, which can further react (as illustrated in Table 2) and be incorporated into the gel. Since the model does not provide the distribution of L_A and other DVB-containing sequences between sol and gel phases, only styrene-made linear chains were considered in the calculation of w_p.

Table 2 Reactions in terms of sequences

Chemical equations		
$R_0^{\cdot} + M_1 \xrightarrow{k_{I_1}} R_S^{\cdot}$	$L_{Ar} + L_{Cs} \xrightarrow{k_t} L_{Dr+s}$	$R_S^{\cdot} + L_{Ar} \xrightarrow{k_t} F$
$R_S^{\cdot} + M_1 \xrightarrow{k_{P_1}} R_S^{\cdot}$	$L_{Ar} + L_{As} \xrightarrow{k_{P3}} L_{Cr} + L_{C0} + L_{Ds}$	$R_S^{\cdot} + L_{Cr} \xrightarrow{k_t} F$
$R_0^{\cdot} + M_2 \xrightarrow{k_{I_2}} L_{A0}$	$L_{Ar} + L_{Bs} \xrightarrow{k_{P3}} L_{Dr} + L_{Ds} + L_{C0}$	$R_S^{\cdot} + L_{Ar} \xrightarrow{k_{P3}} L_{Cr} + L_{C0}$
$R_S^{\cdot} + M_2 \xrightarrow{k_{P_2}} L_{A0}$	$L_{Ar} + L_{Ds} \xrightarrow{k_{P3}} L_{Dr} + L_{Es} + L_{C0}$	$R_S^{\cdot} + L_{Br} \xrightarrow{k_{P3}} L_{Dr} + L_{C0}$
$R_S^{\cdot} + R_S^{\cdot} \xrightarrow{k_t} P$	$L_{Cr} + L_{As} \xrightarrow{k_{P3}} L_{Er} + L_{Cs} + L_{C0}$	$R_S^{\cdot} + L_{Dr} \xrightarrow{k_{P3}} L_{Er} + L_{C0}$
$L_{Ar} + M_1 \xrightarrow{k_{P_1}} L_{Ar+1}$	$L_{Cr} + L_{Bs} \xrightarrow{k_{P3}} L_{Er} + L_{Ds} + L_{C0}$	$R_0^{\cdot} + L_{Ar} \xrightarrow{k_{P3}} L_{Cr} + L_{C0}$
$L_{Ar} + M_2 \xrightarrow{k_{P_2}} L_{Br} + L_{A0}$	$L_{Cr} + L_{Ds} \xrightarrow{k_{P3}} L_{Er} + L_{Es} + L_{C0}$	$R_0^{\cdot} + L_{Br} \xrightarrow{k_{P3}} L_{Dr} + L_{C0}$
$L_{Cr} + M_1 \xrightarrow{k_{P_1}} L_{Cr+1}$	$L_{Cr} + L_{Cs} \xrightarrow{k_t} L_{Er+s}$	$R_0^{\cdot} + L_{Dr} \xrightarrow{k_{P3}} L_{Er} + L_{C0}$
$L_{Cr} + M_2 \xrightarrow{k_{P_2}} L_{Dr} + L_{A0}$	$R_0^{\cdot} + L_{Ar} \xrightarrow{k_t} F$	$L_{Ar} \xrightarrow{k_{cyc}} Cy_r + L_{C0}$
$L_{Ar} + L_{As} \xrightarrow{k_t} L_{Br+s}$	$R_0^{\cdot} + L_{Cr} \xrightarrow{k_t} F$	

$R_0^{\cdot}$: Primary radical, M_1: vinyl monomer (styrene), M_2: divinyl monomer (divinylbenzene—DVB), $R_S^{\cdot}$: polymeric radical containing only styrene units, P: dead polymer, F: polymer fragment, L_{Ar} to L_{Er}: sequences containing r repeating units, Cy_r: cyclic chain containing r units

Including a gelation model would considerably increase the computational effort with limited benefit, as occluded chains do not have a pivotal impact on the prediction of the PCD distribution.

Balance of sequences

The copolymerization model developed herein involves the free radical mechanism also described in terms of sequences. It is the same mechanism displayed in Table 1 but quantifying the sequences formed in the product, as illustrated in Fig. 1 and given in Table 2.

As shown in Fig. 1, different sequences share some groups, which can cause confusion when interpreting the steps in Table 2. At first glance, it may seem impossible to treat the sequences as isolated species since they are connected to other sequences. However, the approach is kinetically consistent because, in reactions involving sequences, the consumption of side sequences is accounted for in other steps of the population balance.

The balances of sequences are described in Eqs. 11–21.

$$\frac{\mathrm{d}R_S^{\cdot}}{\mathrm{d}t} = k_{I1}R_0^{\cdot}M_1 - k_{P2}R_S^{\cdot}M_2 - k_{P3}R_S^{\cdot}\left(\sum_{r=0}^{n_{\max}} L_{Ar} + 2\sum_{r=0}^{n_{\max}} L_{Br} + \sum_{r=0}^{n_{\max}} L_{Dr}\right) - k_t R_S^{\cdot}\left(\sum_{r=0}^{n_{\max}} L_{Ar} + \sum_{r=0}^{n_{\max}} L_{Cr}\right) - k_t {R_S^{\cdot}}^2 \quad (11)$$

$$\frac{\mathrm{d}L_{A0}}{\mathrm{d}t} = k_{I2}R_0^{\cdot}M_2 + k_{P2}M_2\left(\sum_{r=0}^{n_{\max}} L_{Ar} + \sum_{r=0}^{n_{\max}} L_{Cr} + R_S^{\cdot}\right) - L_{A0}\left[k_{P1}M_1 + k_{P2}M_2 + k_t\left(\sum_{r=0}^{n_{\max}} L_{Ar} + \sum_{r=0}^{n_{\max}} L_{Cr} + R_0^{\cdot} + R_S^{\cdot}\right) + k_{P3}\left(2\sum_{r=0}^{n_{\max}} L_{Ar} + 2\sum_{r=0}^{n_{\max}} L_{Br} + \sum_{r=0}^{n_{\max}} L_{Cr} + \sum_{r=0}^{n_{\max}} L_{Dr} + R_0^{\cdot} + R_S^{\cdot}\right)\right] \tag{12}$$

$$\frac{\mathrm{d}L_{Ar}}{\mathrm{d}t} = k_{P1}M_1L_{Ar-1} - k_{P1}M_1L_{Ar} - k_{P2}M_2L_{Ar} - k_tL_{Ar}\left(\sum_{s=0}^{n_{\max}} L_{As} + \sum_{s=0}^{n_{\max}} L_{Cs} + R_S^{\cdot} + R_0^{\cdot}\right) - k_{P3}L_{Ar}\left(2\sum_{s=0}^{n_{\max}} L_{As} + 2\sum_{s=0}^{n_{\max}} L_{Bs} + \sum_{s=0}^{n_{\max}} L_{Cs} + \sum_{s=0}^{n_{\max}} L_{Ds} + R_S^{\cdot} + R_0^{\cdot}\right) - k_{\mathrm{cyc}}L_{Ar} \tag{13}$$

$$\frac{\mathrm{d}L_{B0}}{\mathrm{d}t} = k_{P2}L_{A0}M_2 + \frac{1}{2}k_tL_{A0}^2 - 2k_{P3}L_{B0}\left(\sum_{r=0}^{n_{\max}} L_{Ar} + \sum_{r=0}^{n_{\max}} L_{Cr} + R_0^{\cdot} + R_S^{\cdot}\right) \tag{14}$$

$$\frac{\mathrm{d}L_{Br}}{\mathrm{d}t} = k_{P2}L_{Ar}M_2 + \frac{1}{2}k_t\sum_{s=1}^{r} L_{As}L_{Ar-s} - 2k_{P3}L_{Br}\left(\sum_{s=0}^{n_{\max}} L_{As} + \sum_{s=0}^{n_{\max}} L_{Cs} + R_0^{\cdot} + R_S^{\cdot}\right) \tag{15}$$

$$\frac{\mathrm{d}L_{C0}}{\mathrm{d}t} = -k_{P1}L_{C0}M_1 - k_{P2}L_{C0}M_2 - k_tL_{C0}\left(\sum_{s=0}^{n_{\max}} L_{As} + \sum_{s=0}^{n_{\max}} L_{Cs} + R_S^{\cdot} + R_0^{\cdot}\right) - k_{P3}L_{C0}\left(\sum_{s=0}^{n_{\max}} L_{As} + 2\sum_{s=0}^{n_{\max}} L_{Bs} + \sum_{s=0}^{n_{\max}} L_{Ds}\right) + k_{P3}\sum_{r=0}^{n_{\max}} L_{Ar}\left(2\sum_{r=0}^{n_{\max}} L_{As} + 2\sum_{s=0}^{n_{\max}} L_{Bs} + \sum_{s=0}^{n_{\max}} L_{Cs} + \sum_{s=0}^{n_{\max}} L_{Ds} + R_S^{\cdot} + R_0^{\cdot}\right) + 2k_{P3}\sum_{r=0}^{n_{\max}} L_{Br}\left(\sum_{s=0}^{n_{\max}} L_{Cs} + R_S^{\cdot} + R_0^{\cdot}\right) + k_{P3}\sum_{r=0}^{n_{\max}} L_{Dr}\left(\sum_{s=0}^{n_{\max}} L_{Cs} + R_S^{\cdot} + R_0^{\cdot}\right) + k_{cyc}\sum_{r=3}^{n_{\max}} L_{Ar} \tag{16}$$

$$\frac{\mathrm{d}L_{Cr}}{\mathrm{d}t} = k_{P1}L_{Cr-1}M_1 - k_{P1}L_{Cr}M_1 - k_{P2}L_{Cr}M_2 - k_tL_{Cr}\left(\sum_{s=0}^{n_{\max}} L_{As} + \sum_{s=0}^{n_{\max}} L_{Cs} + R_S^{\cdot} + R_0^{\cdot}\right) - k_{P3}L_{Cr}\left(\sum_{s=0}^{n_{\max}} L_{As} + 2\sum_{s=0}^{n_{\max}} L_{Bs} + \sum_{s=0}^{n_{\max}} L_{Ds}\right) + k_{P3}L_{Ar}\left(\sum_{s=0}^{n_{\max}} L_{As} + \sum_{s=0}^{n_{\max}} L_{Cs} + R_S^{\cdot} + R_0^{\cdot}\right) \tag{17}$$

$$\frac{dL_{D0}}{dt} = k_{P2}M_2L_{C0} + k_tL_{A0}L_{C0} + k_{P3}L_{A0}\left(2\sum_{s=0}^{n_{max}}L_{Bs} + \sum_{s=0}^{n_{max}}L_{Ds} + \sum_{s=0}^{n_{max}}L_{As}\right) + 2k_{P3}L_{B0}\left(\sum_{s=1}^{n_{max}}L_{As} + \sum_{s=0}^{n_{max}}L_{Cs} + R_0^{\cdot} + R_S^{\cdot}\right) - k_{P3}L_{D0}\left(\sum_{s=0}^{n_{max}}L_{As} + \sum_{s=0}^{n_{max}}L_{Cs} + R_0^{\cdot} + R_S^{\cdot}\right) \tag{18}$$

$$\frac{dL_{Dr}}{dt} = k_{P2}L_{Cr}M_2 + k_t\sum_{s=1}^{r}L_{As}L_{Cr-s} + k_{P3}L_{Ar}\left(2\sum_{s=0}^{n_{max}}L_{Bs} + \sum_{s=0}^{n_{max}}L_{Ds} + \sum_{s=0}^{n_{max}}L_{As}\right) + 2k_{P3}L_{Br}\left(\sum_{s=0}^{n_{max}}L_{As} + \sum_{s=0}^{n_{max}}L_{Cs} + R_S^{\cdot} + R_0^{\cdot}\right) - k_{P3}L_{Dr}\left(\sum_{s=0}^{n_{max}}L_{As} + \sum_{s=0}^{n_{max}}L_{Cs} + R_S^{\cdot} + R_0^{\cdot}\right) \tag{19}$$

$$\frac{dL_{E0}}{dt} = k_{P3}\left(L_{C0} + L_{D0}\right)\sum_{s=0}^{n_{max}}L_{As} + k_{P3}L_{C0}\left(2\sum_{s=0}^{n_{max}}L_{Bs} + \sum_{s=0}^{n_{max}}L_{Ds}\right) + k_{P3}L_{D0}\left(\sum_{s=1}^{n_{max}}L_{Cs} + R_0^{\cdot} + R_S^{\cdot}\right) + \frac{1}{2}k_tL_{C0}^2 \tag{20}$$

$$\frac{dL_{Er}}{dt} = k_{P3}\sum_{s=0}^{n_{max}}L_{As}\left(L_{Cr} + L_{Dr}\right) + k_{P3}L_{Cr}\left(2\sum_{s=0}^{n_{max}}L_{Bs} + \sum_{s=0}^{n_{max}}L_{Ds}\right) + k_{P3}L_{Dr}\left(\sum_{s=0}^{n_{max}}L_{Cs} + R_S^{\cdot} + R_0^{\cdot}\right) + \frac{1}{2}k_t\sum_{s=1}^{r}L_{Cs}L_{Cr-s} \tag{21}$$

For explanatory purposes, the terms in Eq. 19 are detailed as follows:

The formation of a sequence containing a cross-linking point and a pendant double bond (PDB) at its ends (L_D) depends on the incorporation of a DVB unit at the radical center of an L_C sequence, represented by the propagation term: $k_{P2}L_{Cr}M_2$.

Termination of radical centers from L_C and L_A sequences also produces L_D, described by the term: $k_t\sum_{s=1}^{r}L_{As}L_{Cr-s}$. The radical center of L_A may undergo cross-linking and become a cross-linking point, thereby transforming L_A into L_D. This is represented by the term: $k_{P3}L_{Ar}\left(2\sum_{s=0}^{n_{max}}L_{Bs} + \sum_{s=0}^{n_{max}}L_{Ds} + \sum_{s=0}^{n_{max}}L_{As}\right)$. The L_D sequence can also be formed by the consumption of a PDB from L_B, accounted for by: $2k_{P3}L_{Br}\left(\sum_{s=0}^{n_{max}}L_{As} + \sum_{s=0}^{n_{max}}L_{Cs} + R_S^{\cdot} + R_0^{\cdot}\right)$.

On the other hand, consumption of L_D sequences occurs when any radical center reacts with the PDB from L_D, which is taken into account by the term: $-k_{P3}L_{Dr}\left(\sum_{s=0}^{n_{max}}L_{As} + \sum_{s=0}^{n_{max}}L_{Cs} + R_S^{\cdot} + R_0^{\cdot}\right)$.

All differential equations were integrated in Scilab through the algorithm ode. The kinetic parameters and synthesis conditions considered in the copolymerization simulations can be found elsewhere [11]. The cyclization reactivities used in the copolymerization simulations were collected from a previous study [14].

Among the five types of sequences, L_{Ar} to L_{Er}, the sequence L_{Er} is directly associated with the chain density of the resin. Having the distribution of sequences, it is possible to calculate the distribution of molecular weights between cross-links (M_{Cr}), as described in Eq. 22.

$$M_{Cr} = M_{\mathrm{Sty}} L_{Er} \tag{22}$$

where M_{Sty} is the molecular weight of styrene.

The mass fraction of a sequence of length r along the polymer network is determined as follows.

$$Y_{rLE} = \frac{rL_{Er}}{\sum_{r=0}^{n_{\max}} rL_{Er}} \tag{23}$$

The calculation for the fraction of other sequences (Y_{rLA} to Y_{rLD}) is analogous to Eq. 23.

An $n_{\max}$ is required for the simulations, which represents the longest sequence considered in the system. It was adopted $n_{\max} = 100$, since higher values provide very similar results.

Swelling behavior

The swelling behavior of resins is influenced by their interaction with the solvent, cross-link density, and other factors. Karam and Tien [15] present a theoretical approach for calculating the swelling index associated with each L_{Er} (Sw_r) of a resin with occlusions in a specific solvent, utilizing a modified Flory–Rehner equation. The associated algorithm is discussed in 24–27.

$$ln\left(1 - v_R\right) + v_R + \mu_R v_R^2 + \frac{\rho_R V_1 v_R^{\frac{1}{3}}}{M_{C_n} K^{\frac{4}{3}}} - \left[ln\left(1 - v_0\right) + v_0 + \mu_P v_0^2\right] = 0 \tag{24}$$

$$\begin{aligned} &ln\left(1 - v_R\right) + v_R + \mu_R v_R^2 + \frac{\rho_R V_1 v_R^{\frac{1}{3}(1+2K^2)}}{3M_{C_n} K^{\frac{4}{3}}} \\ &+ \frac{(K+1)^3 + 2K^3}{2\left[(K+1)^3 - K^3\right]} \left\{ln\left(1 - v_P\right) + v_P + \mu_P v_P^2 - \left[ln\left(1 - v_0\right) + v_0 + \mu_P v_0^2\right]\right\} \end{aligned} \tag{25}$$

$$K = \frac{v_R}{v_P} \tag{26}$$

$$Sw_n = 1 + \frac{\left[\frac{\rho_s}{\rho_R} w_R \left(\frac{1}{v_R} - 1\right) + \frac{\rho_s}{\rho_P} w_P \left(\frac{1}{v_P} - 1\right)\right]}{w_R + w_P} \tag{27}$$

where the interaction parameters can be calculated as follows [16].

$$\mu_R = \mu_P = 0.34 + V_1 \frac{A_{12}}{RT} \tag{28}$$

$$A_{12} = \left(\delta_s - \delta_R\right)^2 \tag{29}$$

The system was initialized with the values of M_{Cr} and w_p provided by the copolymerization model, and with $v_0 = 0$, assuming no dissolved polymer in the supernate. The nonlinear system of Eqs. 24–27, involving four unknowns (v_R, v_P, K and Sw), was solved using the fsolve function in Scilab.

Blanks and Prausnitz (1964) indicated that Eq. 29 is applicable only for apolar–apolar solvent–polymer interactions. For polar–apolar and polar–polar interactions, the term A_{12} is described by different equations [16]. Consequently, instead of determining the solubility parameters (δ), the parameter A_{12} was directly fitted to the studies system.

The density of sulfonated polystyrene (ρ_{PS}) was determined using a method group contribution described by Sewell [17]. In this study, the densities of the resin (ρ_R) and occluded polystyrene (ρ_P) were both considered to be approximately 1.288 g cm^{-3}, as calculated through the aforementioned method.

Polymer chain density prediction

The term Sw_r described in the previous section represents the swelling index of a region with sequences L_{Er}, which have the molecular weight M_{Cr}, as illustrated in Fig. 2.

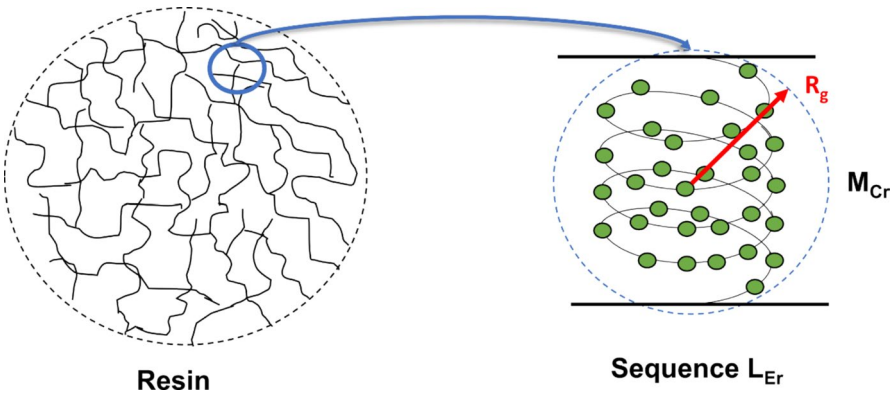

Fig. 2 Pictorial representation of coiling of a sequence L_{Er}

Figure 2 exemplifies the coiling effect which is well known to happen in polymer chains. The radius of gyration (R_g) of polymer chain can be calculated as a function of the molecular weight of the chain, as follows [18].

$$R_g = \beta M_W^{\alpha} \tag{30}$$

where the constant β and the coiling factor α depends on the type of polymer, degree of cross-linking, type of solvent, etc. [18, 19]. For example, $\beta = 0.0123$ and $\alpha = 0.5936$ for polystyrene in toluene at 25 °C [18]. For unperturbed chains in dry state, $\beta = 0.03$ and $\alpha = 0.5$ [20]. Since this information is scarce for sulfonated resins swollen in water, the present work adopted the starting point from an unperturbed system ($\beta = 0.03$) and α was fitting parameters depending on the type of resin. Hence, the radius of gyration for the sequence L_{Er} was defined as follows.

$$R_{g_r} = 0.03 M_{C_r}^{\alpha} \tag{31}$$

The density of a given portion of swollen polymer (φ) is given by Eq. 32.

$$\varphi = \frac{m_p}{V_p + V_s} \tag{32}$$

where m_p, V_p, and V_s are the mass of polymer, volume of polymer, and volume of solvent, respectively.

It is understood that the densities and swelling index are defined as described in Eqs. 33 and 34.

$$\rho_p = \frac{m_p}{V_p}; \rho_s = \frac{m_s}{V_s} \tag{33}$$

$$\mathrm{Sw} = \frac{m_p + m_s}{m_p} \tag{34}$$

Substituting 33 and 34 in 32:

$$\varphi = \frac{1}{\frac{1}{\rho_p} + \frac{Sw-1}{\rho_s}} \tag{35}$$

In Eq. 35, φ is given in g cm^{-3}. In order to convert this term into polymer chain density (PCD_r), information on the sequence containing r units must be considered, as follows.

$$\mathrm{PCD}_r = \frac{\varphi N_A \varnothing_r}{10^{21} M_{Cr}} \tag{36}$$

Hence, the polymer chain density is defined as:

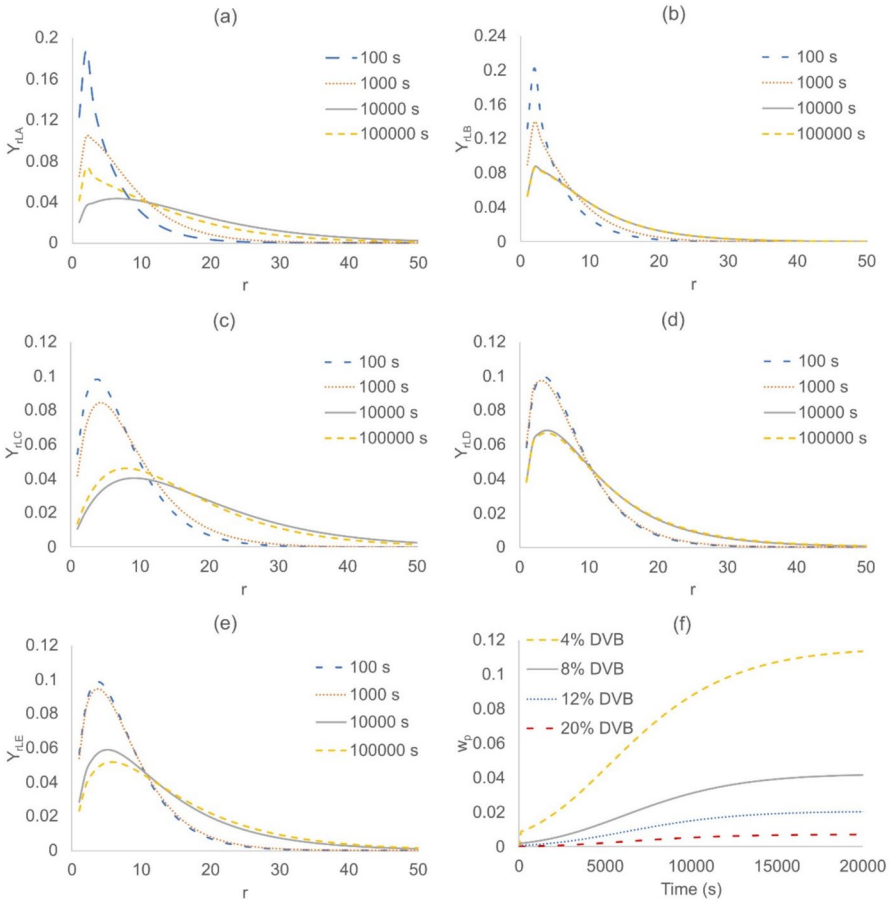

Fig. 3 Copolymerization simulation data. **a**–**e** Time evolution of L_A to L_E distributions, respectively; **f** w_p curves for various DVB feedings. Simulations carried out considering 12% DVB

$$\mathrm{PCD}_r = \frac{602.3\varnothing_r}{M_{Cr}\left(\frac{1}{\rho_p} + \frac{Sw_r - 1}{\rho_s}\right)} \tag{37}$$

where N_A is the Avogadro's number (6.023×10^{23} molecules per mol of sequence), $\varnothing_r$ is the sequence diameter based on the radius of gyration ($\varnothing_r = 2R_{g_r}$) in nm per molecule, 10^{21} is a conversion factor ($\mathrm{nm}^3\ \mathrm{cm}^{-3}$).

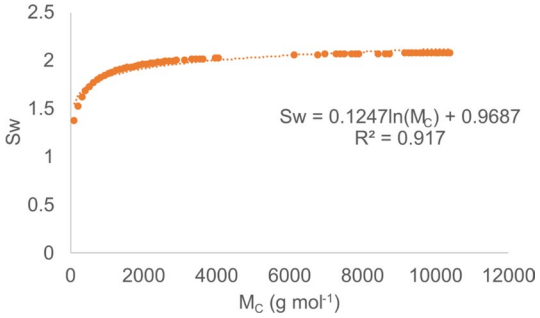

Fig. 4 Swelling index (Sw) as a function of molecular weight between cross-links (M_C). Resin Bayer K 1131 in water. $A_{12} = 49.46$MPa [21]

Table 3 Resin data and simulation parameters

Resin	% DVB	w_p	a	b	α
R1	1.0	0.5300	0.1173	1.0490	0.3040
R2	1.5	0.4100	0.1216	1.0019	0.4678
R3	2.0	0.3300	0.1247	0.9687	0.4900
R4	2.5	0.2700	0.1270	0.9438	0.5304
R5, R6	4.0	0.1600	0.1314	0.8967	0.5907
R7	8.0	0.0518	0.1357	0.8501	0.6518
A16, A36	12.0	0.0211	0.1369	0.8374	0.6436
A15, A35	20.0	0.0056	0.1375	0.8309	0.6121
A46	25.0	0.0029	0.1376	0.8297	0.5809

R1 to R7: resins studied by Jerabek et al. [22] A16 to A46: resins studied by Tejero et al. [23] Optimum values of *a, b* and *α* obtained by the least squares method

Results and discussion

Firstly, simulations were carried out with the copolymerization model in order to observe the behavior of important variables such as sequences distributions and fraction of occluded soluble chains (w_p). Figure 3 illustrates the predicted profiles of the evolution of these variables along the copolymerization.

The high fractions of shorter sequences observed at the early stages of copolymerization (e.g., at 100 s) can be explained by the relatively high concentration of DVB in the medium. The incorporation of DVB into the polymer network leads to the formation of very short sequences (L_{A0}), which subsequently give rise to short L_B to L_E sequences through cross-linking reactions or further incorporation of DVB units.

Conversely, as the copolymerization progresses, the sequence distribution becomes broader due to the depletion of DVB. A slight increase in the L_A distribution profile for shorter sequences is observed at the final stage of the copolymerization. This is attributed to the presence of residual initiator and monomers at a stage

when cross-linking and termination reaction rates are lower, leading to the accumulation of L_A sequences.

The profiles of the fraction of linear chains (w_p) increase with copolymerization time, as expected, since the formation of new chains depends on the availability of initiator fragments (primary radicals), which are also gradually depleted. In addition, higher DVB feed concentrations result in lower w_p profiles. As described in the Mathematical Modeling section, the variable w_p accounts only for styrene-based linear chains. Therefore, the higher the DVB content in the feed, the higher the rate of consumption of these chains due to DVB incorporation.

Cyclization reactions have a slight effect on the concentration of short L_A sequences, but do not significantly affect the L_E sequences.

The set of Eqs. 24–29 were used to collect swelling index data as a function of M_{Cr}. The Sw profile shown in Fig. 4 comprises the range from $M_{C1} = 104.15$ to $M_{C100} = 10415$ g mol^{-1}, representing all the L_{Er} sequences considered in the modeling study.

It is noteworthy that some regions of the profile depicted in Fig. 4 lack data points. This is due to the iterative method used to solve the system of nonlinear Eqs. 24–27. Specifically, this system requires an initial guess, which worked for most of the points, but could not provide satisfactory results for the aforementioned regions. Nevertheless, the data points shown in Fig. 4 were sufficient to allow for curve fitting using a logarithmic function. Due to the numerical issues associated with the system 24–27, the swelling indexes were approximated using logarithmic functions, as follows.

$$\mathrm{Sw}_r = aln\left(M_{Cr}\right) + b \tag{38}$$

where a and b were obtained for each sulfonated resin studied herein by least squares method, providing R^2 values of about 0.92. The resins studied in this work and the respective model parameters are given in Table 3.

Jerabek et al. (2002) analyzed the chain density of the resins R1 to R7, listed in Table 3, which include some commercial products such as Bayer K 1131 (R3), Ostion KSC1 (R5), Amberlyst 31 (R6), and Bayer K 1431 (R7). Similarly, Tejero et al. (2016) analyzed resins from the Amberlyst commercial line: A15, A16, A35, A36, and A46. These resins were selected for study in the present work to compare

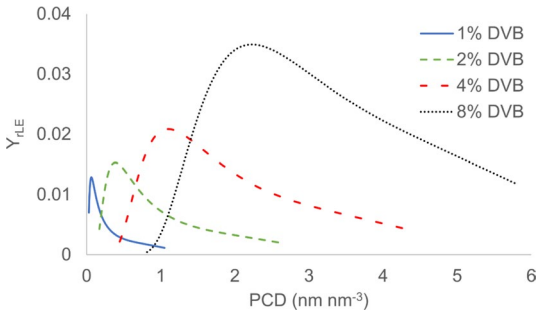

Fig. 5 Polymer chain density (PCD) distributions

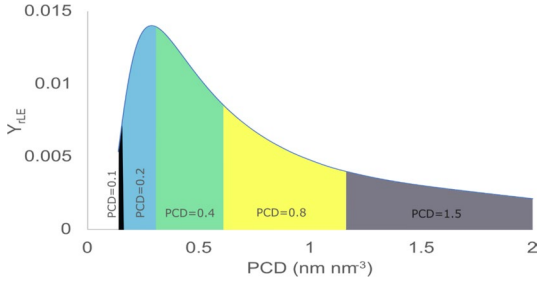

Fig. 6 Discretization of polymer chain densities. Simulation for resin R2

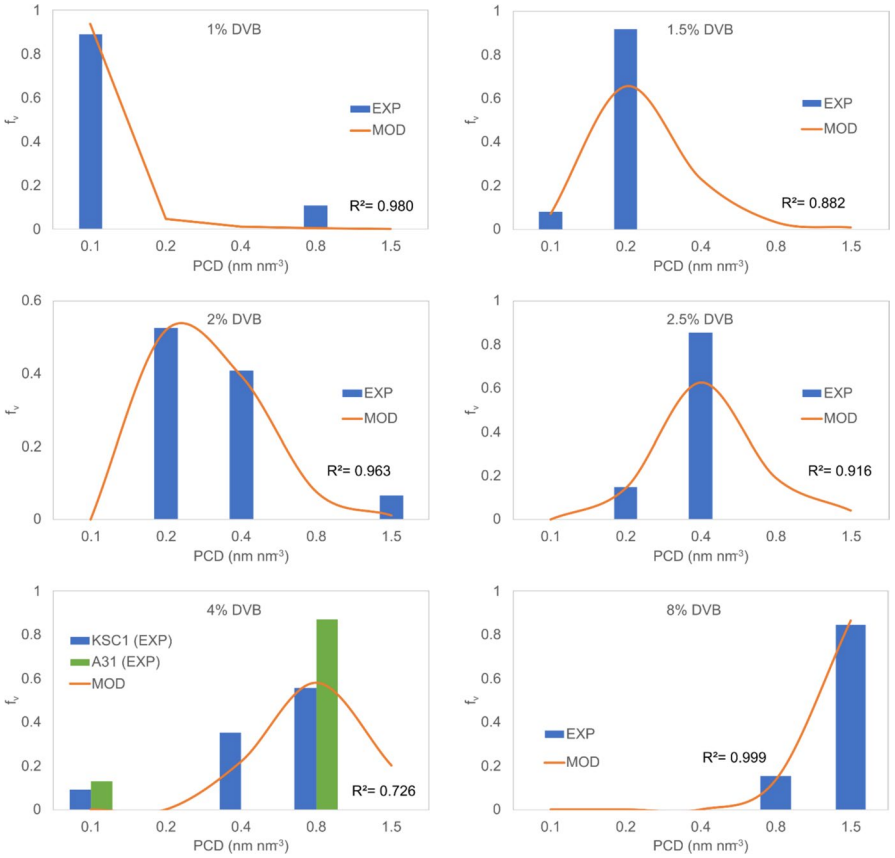

Fig. 7 Model validation with data from Jerabek et al. [22]. *EXP* ISEC experimental data, *MOD* Model predictions

a variety of cross-link densities (different DVB percentages). The values of w_p represent the fraction of linear chains predicted by the model. In the present approach, it was considered that these chains are entrapped within the polymer network. This consideration is feasible for highly cross-linked chains, where the fraction w_p is small and less likely to be removed by washing. Conversely, less cross-linked resins

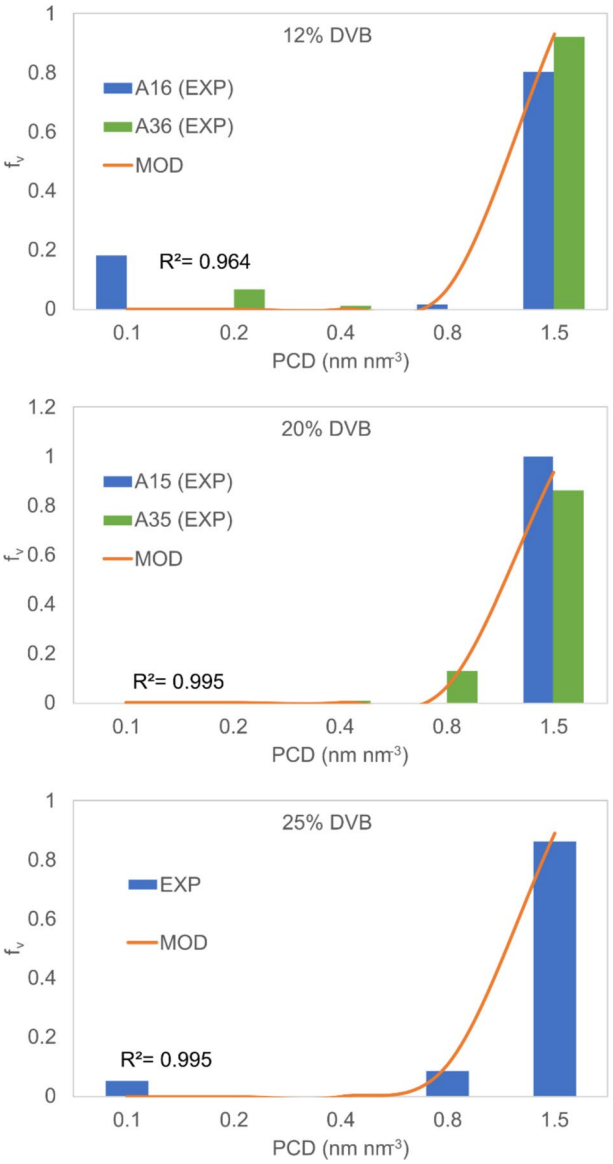

Fig. 8 Model predictions with data from Tejero et al. [23]. *EXP* ISEC experimental data, *MOD* Model predictions

(R1 to R4) are expected to cause less chain entrapment and allow for easier washing, suggesting that the respective predicted w_p values may be overestimated for these cases.

The swelling parameters a and b were used in the PCD simulations with Eq. 37. Figure 5 shows preliminary simulations revealing the effect of DVB percentage on

the polymer chain density distribution of some resins. It is worth noting that Fig. 5 does not represent a probability density function, since Y_{rLE} is plotted against PCD. It would represent a probability density function if plotted against r (see Eq. 23), where the total area under the curve would be equal to one.

Higher densities are observed for higher DVB contents in the resin, as expected. However, the curves shown in Fig. 5 are based on the distribution of sequences, consisting of continuous profiles, while the experimental morphology data of the resin, provided by ISEC, consist of discretized data. Therefore, the PCD profiles obtained from the present simulations were grouped by integrating density regions given by ISEC: 0.1, 0.2, 0.4, 0.8, and 1.5 nm nm^{-3}, as shown in Fig. 6. The boundaries between the colored regions in Fig. 6 were defined as the averages between adjacent regions (i.e., 0.15, 0.3, 0.6, and 1.15). Since the ISEC technique provides discretized data for density regions, the R^2 was calculated by comparing the experimental data with the model results, obtained by integrating the area under each region in Fig. 6.

To validate the present model, we summed the sequence fractions (Y_{rLE}) for each PCD area in Fig. 6. The validation results are presented in Figs. 7 and 8.

In Figs. 7 and 8, f_v represents the fraction of swollen polymer of a specific density (0.1 to 1.5 nm nm^{-3}) relative to the total swollen polymer. The model demonstrates a good ability to represent the chain density distribution of the different resins. The values of α obtained for resins with 4 to 25% DVB are around 0.6, resembling the behavior of polystyrene in toluene [18]. Despite being a sulfonated polystyrene-co-DVB swollen in water, the values fitted for α are not too far off compared to the polystyrene/toluene system for the aforementioned resins. Conversely, resins R2–R4, with DVB contents in the range of 1.5–2.5%, presented behavior similar to that of unperturbed chains ($\alpha \approx 0.5$), which is consistent with the flexibility allowed by the low degrees of cross-linking[1,2]. The coiling factor fitted for resin R1 is significantly lower than for the other cases ($\alpha = 0.3040$). This value may be compensating for aspects not considered in the model, such as the partial removal of soluble chains ($w_p < 0.53$) and the higher reactivity of the cross-linking reaction due to relatively lower entanglements during copolymerization (resulting in fewer hindering effects compared to the synthesis of highly cross-linked resins).

Despite the classified information on the synthesis of the commercial resins, the copolymerization conditions adopted in the present work provided feasible results. This demonstrates that the kinetics of copolymerization is closely linked to the chain density characteristics of ion exchange resins. This kind of study can be refined by synthesizing resins with pre-defined feed compositions under controlled conditions, followed by model validation using variables such as the degree of polymerization, monomer concentration, and morphology data.

Conclusion

The mathematical model developed in this study was successfully validated with morphology data of styrene-based resins cross-linked with 1–25% divinylbenzene (DVB), providing an average R^2 of 0.936. Among the response variables,

the model was able to provide the fraction of linear chains, which decreased with increasing DVB content as expected, and the distribution of sequences between cross-links. This distribution enabled the calculation of swelling index distribution along the resin, which was found to follow a logarithmic function of M_c, yielding an R^2 of approximately 0.920. The positive fitting results indicate that the radius of gyration equation in the form $R_g = 0.03M_{cr}^{\alpha}$ is applicable for chain segments between cross-links (L_{Er}) in sulfonated styrene–DVB resins. For lightly cross-linked sulfonated resins (1.5–2.5% DVB), water could be considered a theta solvent based on the coiling factors found in this work ($\alpha \approx 0.5$). At higher DVB percentages, the coiling behavior of the sequences resembles that of polystyrene in apolar media ($\alpha \approx 0.6$), which is consistent with literature findings. It is important to emphasize that resin morphology depends not only on the monomer proportions but also on the copolymerization conditions. Further studies are warranted to synthesize resins under controlled conditions to refine model predictions regarding polymer chain density and other characteristics.

Acknowledgements This work was supported by the São Paulo Research Foundation (FAPESP)—Grant No. 2024/05061-2.

Author contributions LA wrote the main manuscript text. MR contributed to the illustrations and manuscript revisions. WG was responsible for conceptualization and revisions.

Data availability To foster transparency, the data supporting the findings of this study are derived from previously published experimental results available in the literature. All relevant data and their sources are cited within the manuscript. Any additional data generated during the modeling and analysis process are available from the corresponding author upon reasonable request.

Declarations

Conflict of interest The authors declare that they have no conflict of interest.

References

1. Croxtall B, Hope EG, Stuart AM (2003) Separation, recovery and recycling of a fluorous-tagged nickel catalyst using fluorous solid-phase extraction. Chem Commun 3:2430–2431
2. Biswas K, Ghosh S, Basu B (2020) Ion-exchange resins and polypeptide supported catalysts: a critical review. Curr Green Chem 7:40–52. https://doi.org/10.2174/2213346107666200204125435
3. Soto R, Fité C, Ramírez E, Iborra M, Tejero J (2018) Catalytic activity dependence on morphological properties of acidic ion-exchange resins for the simultaneous ETBE and TAEE liquid-phase synthesis. React Chem Eng 3:195–205
4. Tan JJ, Huang Y, Wu ZQ, Chen X (2017) Ion exchange resin on treatment of copper and nickel wastewater. In: IOP conference series: earth and environmental science, vol 94. Institute of Physics Publishing
5. Cavaco SA, Fernandes S, Quina MM, Ferreira LM (2007) Removal of chromium from electroplating industry effluents by ion exchange resins. J Hazard Mater 144:634–638
6. Barakat MA, Ismat-Shah S (2013) Utilization of anion exchange resin Spectra/Gel for separation of arsenic from water. Arab J Chem 6:307–311
7. Kumar S, Jain S (2013) History, introduction, and kinetics of ion exchange materials. J Chem. https://doi.org/10.1155/2013/957647
8. Sarkar S, Chatterjee PK, Cumbal LH, SenGupta AK (2011) Hybrid ion exchanger supported nanocomposites: sorption and sensing for environmental applications. Chem Eng J 166:923–931
9. Canadell E et al (2024) One-pot liquid-phase synthesis of methyl isobutyl ketone over bifunctional ion-exchange resins: unravelling the role of resins structure and active Pd or Cu phases on sintering, leaching and catalytic activity. Top Catal. https://doi.org/10.1007/s11244-024-01987-9

10. Corain B, Zecca M, Jeřábek K (2001) Catalysis and polymer networks-the role of morphology and molecular accessibility. J Mol Catal A Chem 177:3–20
11. Aguiar LG, Godoy WM, Nápolis L, Faria RPV, Rodrigues AE (2021) Modeling the effect of cross-link density on resins catalytic activities. Ind Eng Chem Res 60:6101–6110
12. Aguiar LG, Godoy WM, Lotufo NM, Graça NABS, Rodrigues AE (2024) Estimation of specific reactivities of commercial gel-type resins through modeling the chain sequences distribution. Chem Eng Commun. https://doi.org/10.1080/00986445.2024.2328572
13. Jeřábek K (1996) Inverse steric exclusion chromatography as a tool for morphology characterization. ACS Symp Ser 635:211–224
14. Aguiar LG et al (2014) Mathematical modeling of NMRP of styrene-divinylbenzene over the pre- and post-gelation periods including cyclization. Macromol React Eng 8:295–313
15. Karam HJ, Tien L (1985) Analysis of swelling of crosslinked rubber gel with occlusions. J Appl Polym Sci 30:1969–1988
16. Blanks RF, Prausnitz JM (1964) Thermodynamics of polymer solubility in polar and nonpolar systems. Ind Eng Chem Fundam 3(1):1–8. https://doi.org/10.1021/i160009a001
17. Sewell JH (1973) A method of calculating densities of polymers. J Appl Polym Sci. https://doi.org/10.1002/app.1973.070170608
18. Teraoka I (2002) Polymer solutions : an introduction to physical properties. Wiley, Hoboken
19. Aguiar LG (2016) Mathematical modeling of the internal surface area of copolymer particles based on elementary gel structures. Macromol React Eng 10:588–599
20. Brandrup J, Immergut EH, Grulke EA (1999) Polymer handbook. Wiley, Hoboken
21. Aguiar L, Author F, Godoy Nuno Graça Alírio Rodrigues W. Resin-catalyzed reaction modeling integrating catalyst swelling and sites accessibility: application to solketal synthesis. Under Review
22. Jeřábek K, Hanková L, Prokop Z, Lundquist EG (2002) Relations between morphology and catalytic activity of ion exchanger catalysts for synthesis of Bisphenol A. Appl Catal A 232:181–188
23. Tejero MA, Ramírez E, Fité C, Tejero J, Cunill F (2016) Esterification of levulinic acid with butanol over ion exchange resins. Appl Catal A Gen 517:56–66